Journal of Applied Polymer Science

Design and optimization of alginate–chitosan–pluronic nanoparticles as a novel meloxicam drug delivery system

Shohreh Fattahpour,[1,2] Morteza Shamanian,[1] Naser Tavakoli,[2,3] Mohammadhossein Fathi,[1,4] Saeid Reza Sheykhi,[2] Shirin Fattahpour[5]

[1]Department of Materials Engineering, Biomaterials Research Group, Isfahan University of Technology, Isfahan 841456-83111, Iran
[2]Isfahan Pharmaceutical Sciences Research Centre, Isfahan University of Medical Sciences, Isfahan 81745-359, Iran
[3]Department of Pharmaceutics, School of Pharmacy, Isfahan University of Medical Sciences, Isfahan, Iran
[4]Dental Materials Research Center, Isfahan University of Medical Sciences, Isfahan, Iran
[5]Department of Biochemistry, Rafsanjan University of Medical Sciences, Rafsanjan, Iran
Correspondence to: S. Fattahpour (E-mail: sh.fattahpour@gmail.com) and N. Tavakoli (E-mail: tavakoli@pharm.mui.ac.ir)

ABSTRACT: The inflammation and pain associated with osteoarthritis are treated with nonsteroidal anti-inflammatory drugs (NSAIDs). This treatment is accompanied by several side effects; therefore local intra articular (IA) NSAID injection can be more efficient and safe than systemic administration or topical use. In this study, alginate–chitosan–pluronic nanoparticles were considered as a new vehicle for IA meloxicam delivery. These novel nanoparticles were prepared using an ionotropic gelation method and were optimized for variables such as alginate to chitosan mass ratio, pluronic concentration, and meloxicam concentration using a 3-factor in 3-level Box-Behnken design. To optimize the formulation, the dependent variables considered were particle size, zeta potential, entrapment efficiency, and mean dissolution time (MDT). The nanoparticles morphology was characterized by FESEM and AFM. The potential interactions of the drug-polymers were investigated by ATR-FTIR and DSC, and the delivery profile of meloxicam from the nanoparticles was obtained. The average particle size of the optimized nanoparticles was 283 nm, the zeta potential was −16.9 mV, the meloxicam entrapment efficiency was 55%, and the MDT was 8.9 hours. The cumulative released meloxicam amount from the composite nanoparticles was 85% at pH 7.4 within 96 h. The release profile showed an initial burst release followed by a sustained release phase. The release mechanism was non-Fickian diffusion. © 2015 Wiley Periodicals, Inc. J. Appl. Polym. Sci. **2015**, *132*, 42241.

KEYWORDS: biomaterials; composites; drug delivery systems

Received 3 September 2014; accepted 17 March 2015
DOI: 10.1002/app.42241

INTRODUCTION

One of the newest areas in pharmaceutical studies is drug delivery system design; specifically, nanoparticle drug delivery systems are an attractive delivery option. A nanoparticle drug delivery system is able to deliver a precise amount of drug to a specified and proper place at a determined and proper time. These nano delivery systems consist of biodegradable polymers, lipids, nanoliposomes, and magnetic nanoparticles.[1,2]

Osteoarthritis is common disease that develops with age and following accidents, and it is treated with systemic nonsteroidal anti-inflammatory drugs (NSAID), i.e., meloxicam, a selective cyclo-oxygenase2 (Cox2) inhibitor. NSAIDs are effective in reducing pain and inflammation, but they are accompanied by several side effects, such as gastrointestinal bleeding, cardiovascular, and renal failure. Therefore, the preparation of an injectable NSAID formulation for the intra articular (IA) route may be more efficient than systemic administration and can reduce drug side effects. Currently, glucocorticoids and hyaluronic acid are available for IA administration.[3–5]

Recently, natural biopolymers, such as alginate and chitosan, have gained more prominence due to their biocompatible, biodegradable, hydrophilic, and protective properties.[6,7] These polymers have many applications in wound healing, cell culture, tissue engineering, drug delivery, and gene delivery.[8–14] Additionally, chitosan has a structure similar to cartilage glycosaminoglycans.[15]

Recently, several studies have been conducted on investigating meloxicam nanoparticles. Shaji and Varkey developed silica-coated solid lipid nanoparticles (SLNs) to evaluate the antioxidant and antiradical effects of meloxicam in the treatment of

Additional Supporting Information may be found in the online version of this article.

rheumatoid arthritis.[16] The meloxicam nanostructure lipid carriers (NLCs) and SLNs were prepared, and the SLNs were then incorporated in carboxymethyl cellulose. This formulation was used for the topical delivery of meloxicam in inflamed skin. Additionally, caprylic acid-based nanoemulsion of meloxicam in carbopol 940 was used for transdermal delivery.[17,18] Kurti *et al.* used nanosized meloxicam with polyvinyl pyrrolidone and sodium hyaluronate for intranasal delivery as a novel route of meloxicam administration.[5] Meloxicam-loaded poly (D,L-lactide-*co*-glycolide) (PLGA) nanoparticles were prepared using salting out and emulsion evaporation methods for the treatment of colon adenocarcinoma cells.[19] Albuquerque *et al.* prepared PLGA and poly (L-lactide) (PLLA) double-walled nanospheres.[20] Ianiski *et al.* reported the neuroprotective effect of meloxicam-loaded poly caprolactone (PCL) nanocapsules in Alzheimer's disease.[21]

The common disadvantages of SLNs are particle growing, unpredictable gelation tendency, drug expulsion and inherent low incorporation rate due to the crystalline structure of the solid lipid.[22] Certain high crystalline materials may cause crystal-induced arthritis; therefore, SLN and PCL may not be an appropriate choice for IA administration.[23] Although PLGA is a biocompatible polymer, it undergoes hydrolysis in the body and produces lactic and glycolic acid, which induce an acidic microenvironment that may, due to the closed avascular and alymphatic space of articular cartilage cause slight local inflammation.[24] Therefore, alginate−chitosan−pluronic nanoparticles are a better option for meloxicam delivery in articular cartilage. Additionally, the easy preparation methods and the lack of organic solvent usage are advantages of these nanoparticles. Moreover of nanoparticle advantages such as easy penetration, cellular uptake and inclusion in bases, nanoparticles have better flow than microparticles in injections. Needle clogging does not occur; therefore, the patient experiences less pain.[25]

The main objectives of this study were the preparation, optimization, and development of an alginate−chitosan−pluronic nanocomposite as a novel carrier for the controlled delivery of meloxicam. The nanoparticle optimization was performed using Box-Behnken design.

MATERIALS AND METHODS

Materials

Sodium alginate of low viscosity, 0.02 Pa s for a 1% solution at 20°C, was purchased from BDH, UK. Chitosan was supplied by Sigma-Aldrich, USA (medium molecular weight: 75–85% degree of deacetylation). Pluronic F127 was obtained from Sigma-Aldrich, USA. Meloxicam was received as a gift sample from Samisaz, Iran. All other chemicals were of analytical grade and were purchased from Merck, Germany.

Preparation of Meloxicam-Loaded Nanoparticles

Nanoparticles were prepared based on ionotropic gelation via the interaction of poly anionic alginate and poly cationic chitosan in mild conditions at room temperature. For this purpose, sodium alginate was dissolved in deionized water and then allowed to rest to precipitate impurities. Chitosan was dissolved in 1% acetic acid under stirring for four hours. Calcium chloride and pluronic were also dissolved in deionized water. Meloxicam was suspended in a mixture of ethanol and deionized water (85 : 15). The nanoparticles were prepared according to a method reported by Rajaonarivony *et al.*[26] For the main formulations, 0.57 mL of different concentrations (0.05, 0.1, and 0.15%) of meloxicam was added to 11.4 mL sodium alginate (0.063%) and stirred; then, 0.68 mL calcium chloride (20 m*M*) and 1.19 mL of different concentrations (0, 0.05, and 0.1%) of pluronic were added dropwise to sodium alginate and meloxicam solution under 1200 rpm stirring. A bath sonicator was used for 60 s to disintegrate the aggregates in the prepared solution. After 15 min, 2.39 mL of different concentrations (0.029, 0.047, and 0.1%) of chitosan was added in the same manner, and stirring was continued for 15 min. This light, opalescent solution was centrifuged at 1100 rpm for 15 min to exclude large aggregates as pellets at the bottom of the vessel. The pH values of the sodium alginate and chitosan solutions were initially adjusted to 5.2 and 4.9, respectively; then, the pH of the final solution was adjusted to 5.

Experimental Design

The use of experimental design enables one to reduce the number of experiments, the amount of materials and the time consumed. A 3-factor, 3-level design with 3 center points was selected using Design Expert® software (Version 7.1.5, Stat-Ease, Minneapolis, MN).

The independent variables were the alginate to chitosan mass ratio (X_1), the pluronic concentration (X_2), and the meloxicam concentration (X_3). The dependent variables were the particle size (Y_1), zeta potential (Y_2), entrapment efficiency (EE) (Y_3), and mean dissolution time (MDT) (Y_4). The independent variables were used to prepare 15 experimental formulations, and the results for Y_1, Y_2, Y_3, and Y_4 are presented in Table I.

Nanoparticles Size, Surface Charge, and Stability

The mean particle size, polydispersity index, and zeta potential of the nanoparticles were obtained using photon correlation spectroscopy (PCS) at 25°C using a 4-mW He-Ne laser beam at 633 nm (Nano-ZS instrument, 3000 HS, Malvern, UK) with a noninvasive backscatter (NIBS2, angle = 173) optic (Worcestershire, UK). For particle size measurements, a 2 mL sample was sonicated for 30 s in a bath sonicator, placed in the analyzer chamber and measured immediately. For zeta potential measurements, 1 mL nanoparticle solution was evaluated using zetasizer. Triplicate samples were analyzed, and the mean value was reported. To study nanoparticle stability, meloxicam nanoparticles were freeze dried using a Christ Alpha 2–4 lyophilizer (Germany) for 48 h. For this purpose, 5% mannitol, a cryoprotectant, was added to a specific amount of nanoparticles. After freeze drying, the samples were laid at room temperature; over 180 days, the particle size, zeta potential, and release were defined.

Nanoparticles Entrapment Efficiency

The EE of the nanoparticles was performed using direct and indirect methods. For the direct method, a specific amount of freeze dried nanoparticles was dispersed in phosphate buffer saline (PBS) solution (pH = 7.4) and was washed by

Table I. The Observed Responses in Box–Behnken Design for Meloxicam Polymeric Nanoparticles

Formulation	Alginate to chitosan mass ratio: X_1	Pluronic concentration: X_2 (%)	Meloxicam concentration: X_3 (%)	Particle size: Y_1 (nm) (mean ± SD	Zeta potential: Y_2 (mV) (mean ± SD)	Entrapment efficiency: Y_3(%) (mean ± SD)	Mean dissolution time: Y_4(h) (mean ± SD)
1	3.00	0.00	0.10	332 ± 31	−25.1 ± 1.3	14 ± 2	18 ± 0.1
2	10.00	0.00	0.10	247 ± 14	−21.6 ± 2.4	22 ± 1	16 ± 0.3
3	3.00	0.10	0.10	428 ± 42	−24.2 ± 1.2	25 ± 3	16 ± 0.4
4	10.00	0.10	0.10	275 ± 17	−19.6 ± 1.6	20 ± 1	17 ± 0.5
5	3.00	0.05	0.05	375 ± 15	−24.4 ± 1.9	37 ± 2	12 ± 0.3
6	10.00	0.05	0.05	265 ± 23	−19.6 ± 1.3	40 ± 3	11 ± 0.2
7	3.00	0.05	0.15	410 ± 18	−22.3 ± 2.1	10 ± 0	21 ± 0.2
8	10.00	0.05	0.15	321 ± 25	−20.8 ± 2.3	20 ± 2	19 ± 0.5
9	6.50	0.00	0.05	315 ± 14	−23.7 ± 1.9	34 ± 2	13 ± 0.1
10	6.50	0.10	0.05	319 ± 19	−20.4 ± 1.2	37 ± 4	11 ± 0.3
11	6.50	0.00	0.15	347 ± 26	−19.1 ± 1.5	10 ± 1	20 ± 0.4
12	6.50	0.10	0.15	446 ± 27	−22.3 ± 2.4	18 ± 2	20 ± 0.5
13	6.50	0.05	0.10	253 ± 18	−17.2 ± 1.0	55 ± 3	9 ± 0.1
14	6.50	0.05	0.10	276 ± 16	−18.2 ± 0.8	45 ± 3	12 ± 0.1
15	6.50	0.05	0.10	257 ± 14	−16.2 ± 1.1	51 ± 2	10 ± 0.2

centrifuging using a Sigma laboratories centrifuge (Germany) at 18,000 rpm at 4°C for 20 min. Then, the nanoparticles were dispersed in PBS solution (pH = 8) and vortexed 24 h.[27,28] The dispersion was centrifuged using the same conditions, and the absorbance of the supernatant solution was determined using UV spectrophotometer (Shimadzu, Japan) at 369 nm. A blank sample was made from nanoparticles without loaded drug. Absorbance of blank sample was subtracted from absorbance of the loaded nanoparticles to find the final concentration of drug. The EE was calculated as follows:

$$\mathrm{EE} = \frac{weight\ of\ the\ loaded\ meloxicam}{weight\ of\ the\ total\ meloxicam} \times 100 \quad (1)$$

The indirect measurement was obtained by centrifuging nanoparticles using the above conditions and reading the UV absorbance of the supernatant solution.[1,29] The amount of loaded meloxicam is the difference between the total amount of meloxicam and the amount in the supernatant. The EE was calculated as follows:

$$\mathrm{EE} = \frac{weight\ of\ the\ total\ meloxicam - weight\ of\ the\ free\ meloxicam}{weight\ of\ the\ total\ meloxicam} \times 100 \quad (2)$$

Optimization, Data Analysis, and Model Validation

The ANOVA test in the Design Expert® software was used for data analysis and statistical validation. The observed responses were fitted to linear, second order and quadratic models and were evaluated for statistical significance and R^2 values. Three optimum checkpoint formulations were prepared to evaluate the experimental domain and polynomial equations, and the obtained results were compared with the predicted values.

Nanoparticles Morphology

The morphological analysis of the nanoparticles was performed using field emission scanning electron microscopy (FESEM). The samples were mounted on an aluminum sheet, coated with a thin layer of gold under a vacuum, and observed using a S4160, Hitachi, Japan, FESEM. Atomic force microscopy (AFM) was also used to study the surface morphology, three-dimensional arrangement, and association of the nanoparticles. The image measurement was performed in tapping mode using a silicon probe cantilever of 450 μm length, with an 8−10 nm tip radius of curvature. A minimum of 10 images from each sample were analyzed to assure reproducible results. One milliliter of nanoparticle solution was diluted with 0.5 mL deionized water. Then, one drop of the diluted nanoparticle solution was dried on a layer, the AFM image was obtained using a NANOS 1.1 Bruker, Germany, and the image was processed and analyzed using the Image Plus software program.

Attenuated Total Reflectance Fourier Transform Infrared Spectroscopy (ATR-FTIR)

The ATR-FTIR spectra of the lyophilized nanoparticles were recorded on an FTIR spectrometer with ATR accessories (Tensor27, Bruker, Germany). All spectra were obtained using 16 scans and 1 cm^{-1} resolution. The sampling accessory was a Pike Technologies (Madison, WI) Miracle AG horizontal ATR

accessory equipped with a Zn-Se crystal. All spectra were obtained with the clamp pressure set to its maximum value. The "powder funnel" arrangement of the ATR accessory was used during these experiments. It was found that a minimal amount of material, only just enough to cover the crystal surface, maximized the absorbance values. For this propose, a sample of nanoparticles was scanned over the wavelength range of 600−4000 cm^{-1}.

Differential Scanning Calorimetry (DSC)

DSC thermograms were performed using a thermal analyzer (Mettler, Switzerland). The nanoparticles were lyophilized, and specific amounts were crimped in a standard aluminum pan and heated from 25 to 400°C at a constant heating rate of 10°C/min under nitrogen purge.

In Vitro Drug Release Studies

Two milliliters of meloxicam-loaded nanoparticles solution were placed in a dialysis membrane (molecular weight cutoff 12 KD) and immersed in 10 mL PBS containing 0.5% Tween 20, pH 7.4. The mixture was then stirred in an incubator shaker (Daiki, Korea) at 50 rpm and 37.0 ± 0.1°C. The medium was replaced at the first hour to remove any unloaded drug. At predetermined time intervals, a 2 mL aliquot was withdrawn and analyzed for drug concentration using an UV spectrophotometer at 369 nm. To assure that the sinking was adequate and to prevent medium turbidity, the whole release medium was withdrawn each day and replaced with fresh medium.

Release Kinetics

The obtained release profiles were fitted into four classical mathematical models including Zero order ($m_0 - m = kt$), First order (Ln $m = kt$), Higuchi model ($m_0 - m = kt^{1/2}$) and Hixon-Crowell ($m_0^{1/3} - m^{1/3} = kt$), where m_0 is the initial drug amount, m is the remaining amount of drug, k is the rate constant, and t is the time. The regression coefficient (r) value of each model indicates the appropriateness of the data into the preferred kinetic model. To describe the drug release mechanism from the nanoparticles, the Korsmeyer-Peppas equation was employed, as shown by the following equation:

$$\mathrm{Log}M_t/M_\infty = \log k + n\log t \quad (3)$$

where M_t/M_∞ is the fraction of the released drug at time t, k is the release rate constant, and n is the release exponent, indicating the release mechanism.[30]

RESULTS AND DISCUSSION

Preparation of Meloxicam-Loaded Nanoparticles

Ping Li *et al.* reported an appropriate entrapment of nifedipine into a hydrophilic system by dissolving the drug in a mixture of alcohol and water (1 : 1). The Tyndall effect was observed when the nifedipine nanocrystals were obtained and the suspension of nifedipine nanocrystals was entrapped in the nanoparticles.[31] These findings are consistent with our results because our results showed that meloxicam was suspended in a mixture of alcohol-water and the Tyndall effect was observed after addition to the alginate solution. The solubility and, hence, the entrapment of meloxicam were increased by adding pluronic F127, a nonionic biocompatible copolymer consisting of poly (ethylene oxide)-poly (propylene oxide)-poly (ethylene oxide). Pluronics have been applied in drug delivery to increase the solubility of hydrophobic drugs and to increase the biocompatibility of biomaterials by reducing protein adsorption. Pluronic is a thermo-responsive polymer due to the presence of hydrophobic propylene oxide blocks.[32–35] In a study investigating curcumin encapsulation, Das *et al.* reported a 5- to 10-fold increase in drug entrapment by adding pluronic to the formulation.[36]

The role of pH appears to be important during nanoparticle preparation. It is known that pH provides a contrary charge for the alginate and chitosan, which allows the formation of nanoparticles and affects particle size. Depending on its source and the type of salt, alginate has a pKa within the range of 3.4−4.4, and as the pH approaches 4.5, a large portion of the polymer begins to precipitate.[37] The same phenomenon occurs with chitosan (pKa 6.5), which begins to precipitate at a pH of approximately 5.5.[6,38] Therefore, pH 5, at which the carboxyl groups of alginate were ionized and the amine groups of chitosan were protonated, proved suitable for obtaining the highest amount of polymer interaction and the smallest particle size for the nanoparticles.

The nanoparticles size and zeta potential after freeze drying are presented in Supporting Information Table S1. The particle size was slightly increased after freeze drying. This observation may be due to the nanoparticle agglomeration; however, with increased in storage time, the size was not significantly altered. The zeta potential and meloxicam release profile were not changed.

Model Fitting

The size range of nanoparticles was between 247 and 446 nm. The zeta potential of the nanoparticles was between −16.2 and −25.1 mV. This negative surface charge of the nanoparticles may be due to the alginate carboxyl groups. The EE obtained from the direct and indirect methods did not have significant differences. The maximum EE was estimated to be 55%, and the minimum EE was 10%. Due to the hydrophobic nature of meloxicam, a low EE was expected. This finding was in agreement with previous reports that demonstrated that the EE of oregano essential oil determined using an UV spectrophotometer, ranged from ∼5 to 24.[11] The MDT was between 9 and 21 h. The ratio of maximum to minimum for the responses Y_1, Y_2, Y_3, and Y_4 was 1.8, 1.5, 5.5, and 2.3, respectively. If the ratio of the maximum to minimum response is greater than 10, a model power transformation is necessary.[39]

The values of the coefficients for X_1, X_2, and X_3 relate to the effects of these factors and their comparative significance on the responses. A positive value indicates a synergistic effect between the factor and response, while a negative value indicates an antagonistic effect.[39,40] The regression equations of the fitted models are shown in eqs. (4)−(7).

$$\begin{aligned}\text{Particle size } (Y_1) = {} & 262.00 - 54.62X_1 + 28.38X_2 + 31.25X_3 \\ & - 17.00X_1X_2 + 5.25X_1X_3 + 23.75X_2X_3 + 22.25X_1^2 \\ & + 36.25X_2^2 + 58.5X_3^2\end{aligned} \quad (4)$$

Table II. The ANOVA for the Regressive Models of (a) Particle Size, (b) Zeta Potential, (c) EE, and (d) MDT

Source	Sum of squares	df	Mean Square	*F* Value	*P*-value Prob > *F*	
(a)						
Model	58922.35	9	6546.92	29.09	0.0009	Significant
X_1	23871.12	1	23871.12	106.07	0.0001	Significant
X_2	6441.12	1	6441.12	28.62	0.0031	Significant
X_3	7812.5	1	7812.5	34.71	0.0020	Significant
$X_1 X_2$	1156	1	1156	5.13	0.0728	
$X_1 X_3$	110.25	1	110.25	0.48	0.5152	
$X_2 X_3$	2256.25	1	2256.25	10.02	0.0249	Significant
X_1^2	1827.92	1	1827.92	8.12	0.0358	Significant
X_2^2	4851.92	1	4851.92	21.55	0.0056	Significant
X_3^2	12636	1	12636	56.14	0.0007	Significant
Residual	1125.25	5	225.05			
Lack of Fit	823.25	3	274.41	1.81	0.3742	Not significant
Pure Error	302	2	151			
Cor Total	60047.6	14				
(b)						
Model	99.09	9	11.01	14.52	0.0044	Significant
X_1	25.92	1	25.92	34.19	0.0021	Significant
X_2	1.125	1	1.12	1.48	0.2775	
X_3	1.62	1	1.62	2.13	0.2036	
$X_1 X_2$	0.30	1	0.30	0.39	0.5553	
$X_1 X_3$	2.72	1	2.72	3.59	0.1166	
$X_2 X_3$	10.56	1	10.56	13.93	0.0135	Significant
X_1^2	31.32	1	31.32	41.32	0.0014	Significant
X_2^2	23.30	1	23.30	30.74	0.0026	Significant
X_3^2	10.20	1	10.20	13.46	0.0145	Significant
Residual	3.79	5	0.75			
Lack of Fit	1.79	3	0.59	0.59	0.6754	Not significant
Pure Error	2	2	1			
Cor Total	102.88	14				
(c)						
Model	2918.73	9	324.30	24.69	0.0013	Significant
X_1	32	1	32	2.43	0.1793	
X_2	50	1	50	3.80	0.1085	
X_3	1012.5	1	1012.5	77.09	0.0003	Significant
$X_1 X_2$	42.25	1	42.25	3.21	0.1328	
$X_1 X_3$	12.25	1	12.25	0.93	0.3785	
$X_2 X_3$	6.25	1	6.25	0.47	0.5210	
X_1^2	728.00	1	728.00	55.43	0.0007	Significant
X_2^2	950.16	1	950.16	72.34	0.0004	Significant
X_3^2	336.16	1	336.16	25.59	0.0039	Significant
Residual	65.66	5	13.13			
Lack of Fit	15	3	5	0.19	0.8908	Not significant
Pure Error	50.66	2	25.33			
Cor Total	2984.4	14				
(d)						
Model	236.18	9	26.24	47.71	0.0003	Significant
X_1	2	1	2	3.63	0.1148	

Table II. *Continued*

Source	Sum of squares	df	Mean Square	*F* Value	*P*-value Prob > *F*	
X_2	1.125	1	1.125	2.04	0.2121	
X_3	136.12	1	136.12	247.5	< 0.0001	Significant
$X_1 X_2$	2.25	1	2.25	4.09	0.0990	Significant
$X_1 X_3$	0.25	1	0.25	0.45	0.5301	
$X_2 X_3$	1	1	1	1.81	0.2354	
X_1^2	39	1	39	70.90	0.0004	Significant
X_2^2	45.23	1	45.23	82.23	0.0003	Significant
X_3^2	23.07	1	23.07	41.95	0.0013	Significant
Residual	2.75	5	0.55			
Lack of Fit	0.75	3	0.25	0.25	0.8576	Not significant
Pure Error	2	2	1			
Cor Total	238.93	14				

$$\text{Zeta potential } (Y_2) = -17.20 + 1.8X_1 + 0.37X_2 + 0.45X_3 + 0.28X_1X_2 - 0.82X_1X_3 - 1.63X_2X_3 - 2.91X_1^2 - 2.51X_2^2 - 1.66X_3^2 \quad (5)$$

$$\text{EE } (Y_3) = 50.33 + 2.00X_1 + 2.50X_2 - 11.25X_3 - 3.25X_1X_2 + 1.75X_1X_3 + 1.25X_2X_3 - 14.04X_1^2 - 16.04X_2^2 - 9.54X_3^2 \quad (6)$$

$$\text{MDT } (Y_4) = 10.00 - 0.5X_1 - 0.38X_2 + 4.13X_3 + 0.75X_1X_2 - 0.25X_1X_3 + 0.5X_2X_3 + 3.25X_1^2 + 3.5X_2^2 + 2.5X_3^2 \quad (7)$$

If X_1 is increased, Y_1 will decrease because all of the chitosan compeletly reacted with alginate; therefore, a vigorous interaction occurred, and a small particle size was obtained. Increasing X_1 led to decreased absolute value of Y_2. An increase in X_3 led to an increase in Y_1, Y_4, and a decrease in Y_3. The latter could be due to the bounded capacity of the polymer for drug encapsulation.[41]

The statistical significance of the model terms was defined via an ANOVA analysis (Table II). The reliability of the fitted model was proven by the high *F* values and the low probability values. The ANOVA results demonstrated that particle size was significantly affected by X_1, X_2, and X_3 but that zeta potential was only affected by X_1. Additionally, the EE and MDT were significantly affected by X_3. Based on the analysis offered by the software, the best fitted model was the quadratic model for all of the responses. The comparative values of R^2, adjusted R^2, predicted R^2, *P* value, SD, and CV % are presented in Supporting Information Table S2. For a well-fitted model, the R^2 should not be less than 80%. Coefficients with an R^2 closest to 1 and a *P*-value less than 0.05 had significant effects on the prediction efficacy of the model for the measured response.[42] The R^2 for Y_1, Y_2, Y_3, and Y_4 was 0.9873, 0.9632, 0.9780, and 0.9885, respectively. It is more appropriate to have an adjusted R^2 over 90% to indicate model adequacy.[43] The adjusted R^2 value represents how well the data points fit a statistical model. The values of the predicted and adjusted R^2 for the responses were in reasonably good agreement. Adequate precision measures the signal to noise ratio, a ratio greater than 4 is desirable. The adequate precision values were 15.38, 10.76, 13.71, and 17.54 for Y_1, Y_2, Y_3, and Y_4, respectively. The lack of fit *P*-values was 0.3742, 0.6754, 0.8908, and 0.8576 for Y_1, Y_2, Y_3, and Y_4, respectively. These results implied that the lack of fit, an undesirable factor, was not significant and that the model has nonrepresented data.[44]

Figure 1(a) shows the internally studentized residuals for EE. This plot checks for lurking variables that may influence the response during the experiment, thereby demonstrating the fitness of the model. All of the data points were scattered and laid within the limits. Figure 1(b) shows the DFBETAS for the intercept versus the run number of EE. DFBETAS measures the observation influence on each regression coefficient. This parameter indicates that no observation has considerable influence on the regression coefficient and that there are no data outliers.

Response Surface Plots

Three-dimensional response surface plots are shown in Figures 2 and 3. These plots are useful to investigate the interactions of the factors on the responses. In these figures, two factors are varied, while the third factor is set at a mid-constant level.

Response 1 (Y_1): Effect on Particle Size

The middle concentration of X_2 and an increase in X_1 led to low particle sizes [Figure 2(a)]. Generally, it has been reported that particle size decrease when the surfactant increases, but Xing *et al.* observed that the size of 5-fluorouracil nanoparticles increased when poloxamer increased.[32] We observed that particle size was decreased by a low pluronic concentration, and it then increased. It was apparent that there was an optimal pluronic concentration. This optimal pluronic concentration was near the pluronic critical micelle concentration. It was also demonstrated that low particle sizes were obtained with medium amounts of X_2 and X_3 [Figure 2(b)].

Response 2 (Y_2): Effect on Zeta Potential

With increasing X_1 the absolute zeta potential value initially decreased and then increased [Figure 2(c)]. At the lowest

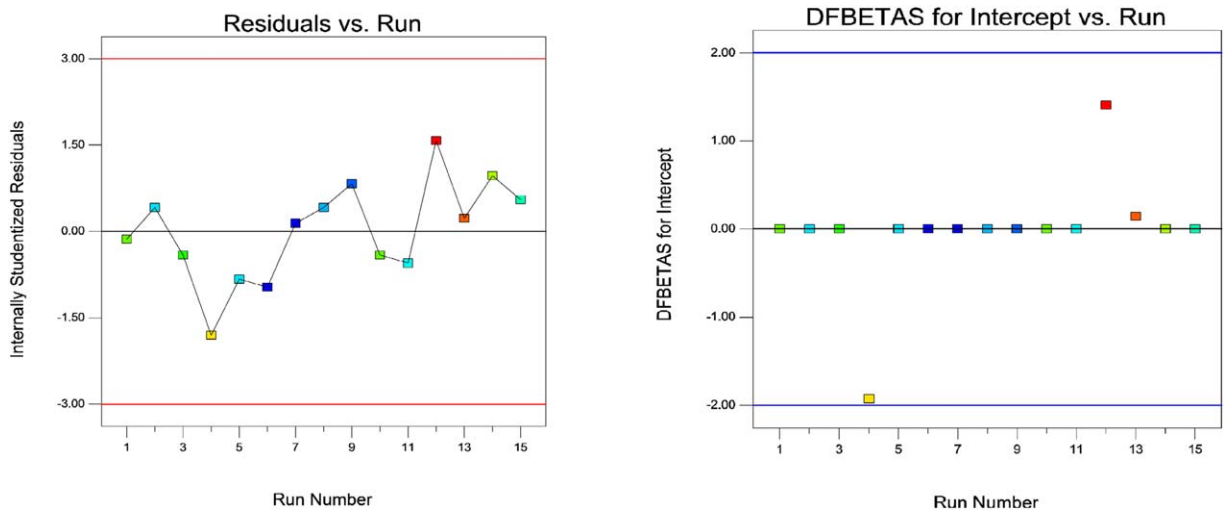

Figure 1. Diagnostic plots for the model adequacy, (a) internally studentized entrapment efficiency residuals versus run number and (b) DFBET for entrapment efficiency intercept versus run number. [Color figure can be viewed in the online issue, which is available at wileyonlinelibrary.com.]

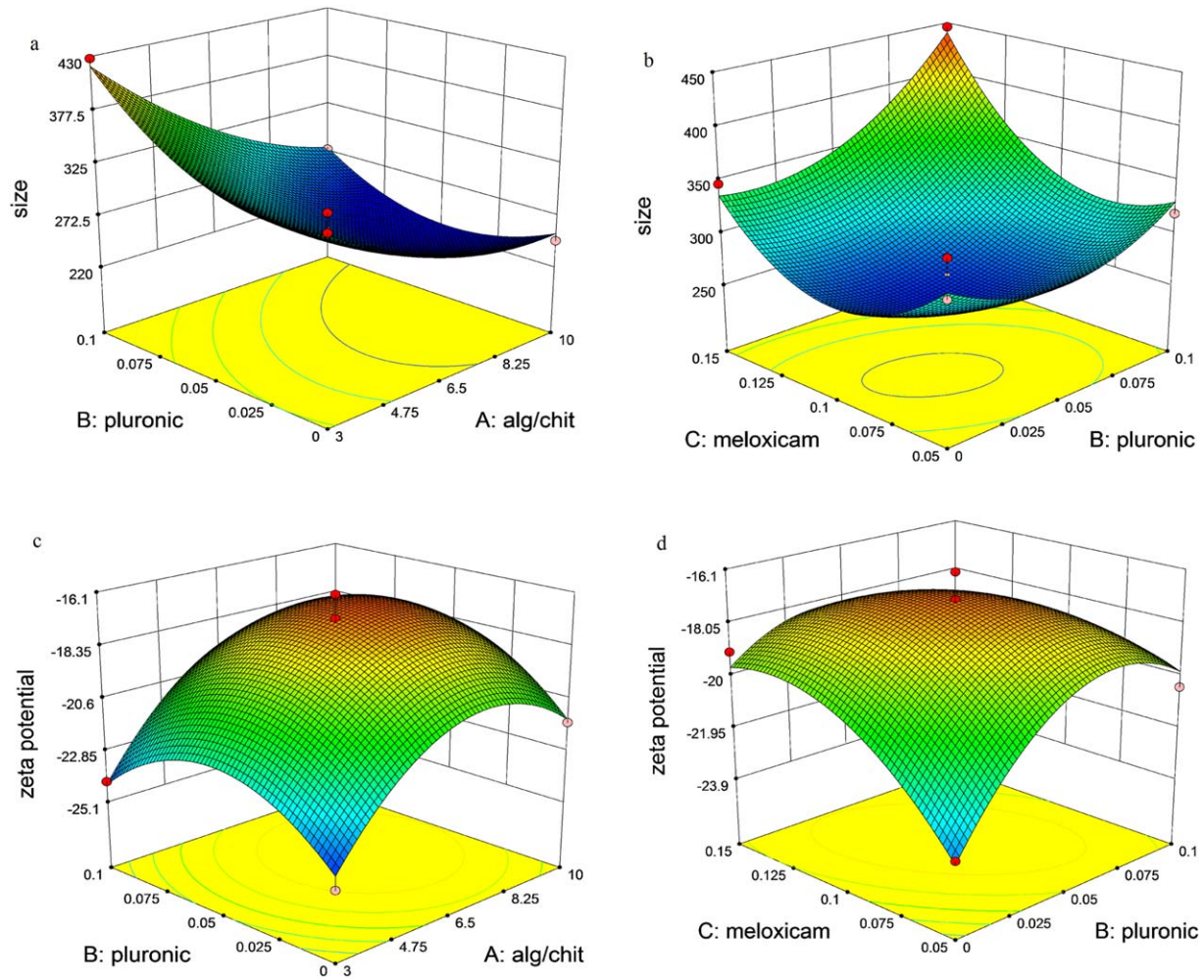

Figure 2. Response surface plots showing the effect of A and B on (a) particle size, (c) zeta potential, B and C on (b) particle size and (d) zeta potential. (A) Alginate to chitosan mass ratio, (B) pluronic concentration, (C) meloxicam concentration. [Color figure can be viewed in the online issue, which is available at wileyonlinelibrary.com.]

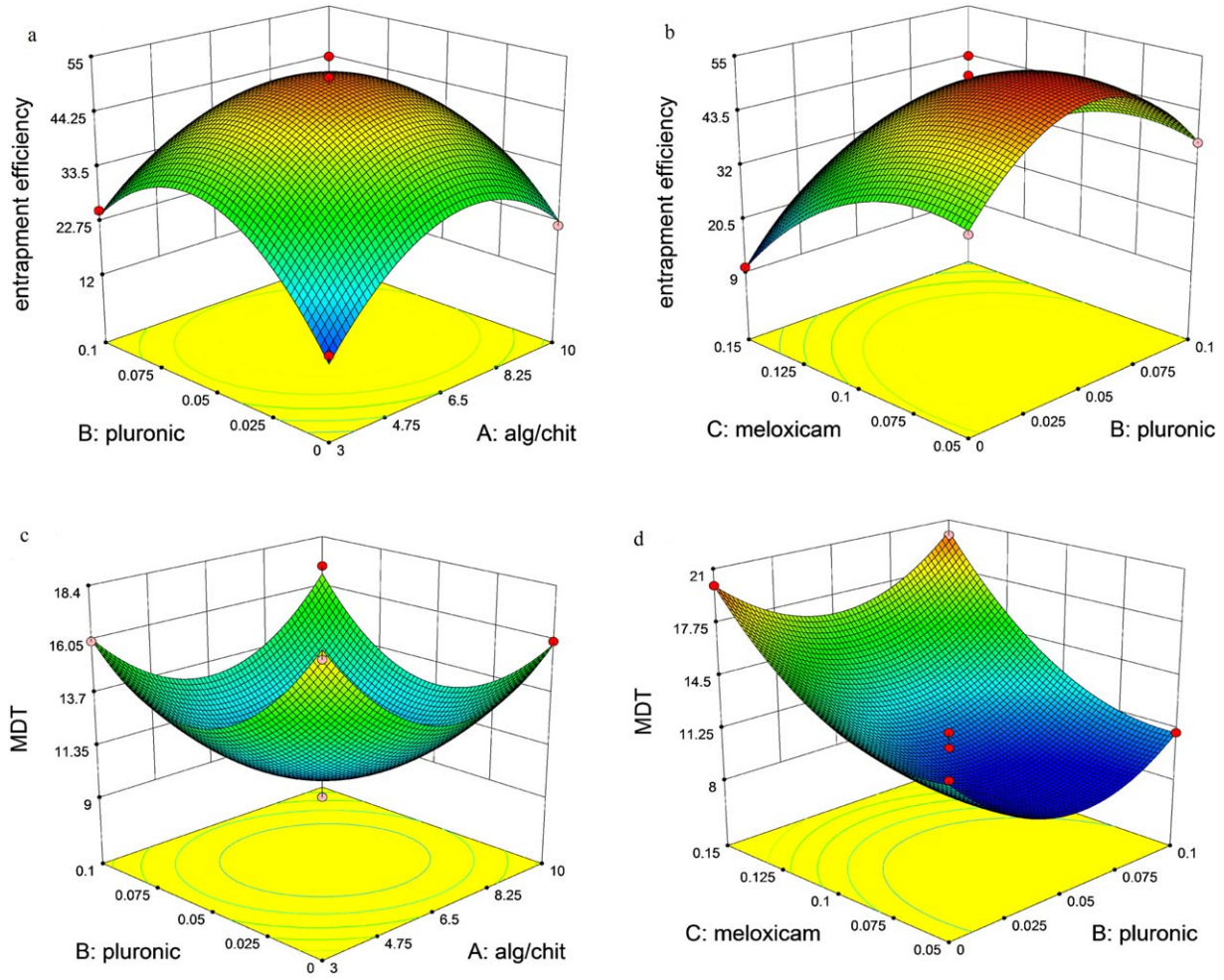

Figure 3. Response surface plots showing the effect of A and B on (a) EE, (c) MDT, B and C on (b) EE and (d) MDT. (A) Alginate to chitosan mass ratio, (B) pluronic concentration, (C) meloxicam concentration. [Color figure can be viewed in the online issue, which is available at wileyonlinelibrary.com.]

absolute zeta potential value, alginate, and chitosan wholly interacted with each other, but in cases that were lower and higher than this area, excessive alginate induced a negative zeta potential. At the medium concentration of X_2, the highest absolute zeta potential value was obtained with the lowest X_3 [Figure 2(d)].

Response 3 (Y_3): Effect on EE

For high entrapment efficiency at high X_1, X_2 must be increased [Figure 3(a)]. Mid X_2 and less than middle X_3 led to high EE [Figure 3(b)]. It has been reported that EE is greatly influenced by drug loading, which is consistent with our finding.[41]

Response 4 (Y_4): Effect on MDT

For a low MDT, X_1, and X_2 must be set at the middle values [Figure 3(c)]. The mid X_2 and less than middle concentration of X_3 led to low MDTs [Figure 3(d)].

The MDT value is used to characterize the drug release rate from a dosage form. According to eq. (8), MDT was strongly related to X_3, and reduced X_3 could reduce MDT, which indicates more release. This agrees with the finding reported by Hosseini *et al.* regarding the encapsulation of oregano essential oil in chitosan nanoparticles. The authors showed that the release profile was related to drug concentration, which was related to the particle size, and a smaller particle size was obtained with low content oregano essential oil nanoparticles.[11] The reduction of meloxicam concentration caused decreased particle size, which may result in a greater surface to volume ratio and would result in an additional release of the meloxicam adsorbed on the nanoparticle surface. Additionally, Shalviri *et al.* reported reduced doxorubicin release by increasing the loading content. The authors explained that the size and surface charge of the particles decreased after drug loading. Doxorubicin is a hydrophobic drug, and the hydrophobicity of the nanoparticles increased with increasing doxorubicin loading content, resulting in lower swelling and release rates.[45] Similar results were observed in our study because meloxicam is a hydrophobic drug as well, and increasing the meloxicam concentration can reduce the zeta potential [Figure 2(d)], increase MDT and reduce the amount of released drug [Figure 3(d)]. These results are apparent in Figure 4.

Optimization and Validation

The optimum nanoparticle formulation was developed based on the following criteria: attaining a particle size and zeta potential

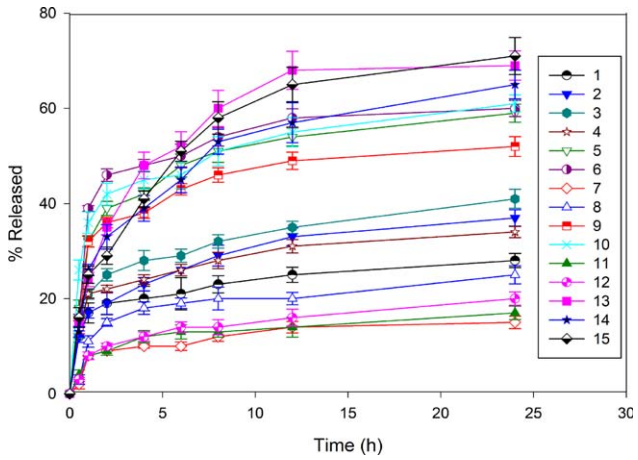

Figure 4. *In vitro* meloxicam release of 15 formulations in PBS and 0.5% Tween 20, pH 7.4, ($n = 3$, bars represent SD). [Color figure can be viewed in the online issue, which is available at wileyonlinelibrary.com.]

from 247 to 446 nm and −16- −25 mV, respectively, the maximal EE value and the minimal MDT value. For the three checkpoint formulations, the results of the evaluation of particle size, zeta potential, EE, and MDT are shown in Table III. All the results were within the acceptable limits, in agreement with each other and had an acceptable percentage prediction error, varying between −7.4 and 5.9%. The predicted versus actual graphs are shown in Supporting Information Figure S1. The linear correlation between the predicted and actual values demonstrates the high prognostic ability of the model. The formulation composition with an alginate to chitosan mass ratio of 6.6, pluronic concentration of 0.05% and meloxicam concentration of 0.05%, was selected as the optimal formulation.

Nanoparticles Morphology, ATR-FTIR, and DSC Analysis

The AFM micrographs of the nanoparticles showed a partly spherical shape, but the FESEM micrographs showed irregular nanoparticles, which may be due to nanoparticle agglomeration according to their zeta potential. Due to the high surface to volume ratio of nanoparticles, their stability is related to their surface charge. If the particle zeta potential value is large, the system will be stable. Conversely, if the zeta potential is relatively small, the system will precipitate.[1] In the AFM micrographs, a dilution of the prepared solution may have caused better separation of the nanoparticles [Figure 5(a, b)].

The ATR-FTIR spectra of alginate, chitosan, meloxicam, and nanoparticles were analyzed to characterize the potential nanoparticle interactions [Figure 6(a)]. In the alginate spectrum, a broad band at 3423 cm^{-1} was attributed to hydroxyl groups, and the peaks at 1612 cm^{-1} and 1414 cm^{-1} were created by symmetric and asymmetric stretching vibrations of COO^{-} groups. The peak near 1030 cm^{-1} corresponded to a saccharide structure. Chitosan had a broad band at 3415 cm^{-1} for the amine groups, a band at 1653 cm^{-1} for the amide groups, a peak at 1379 cm^{-1} for the N—H stretching of the amide-ether bonds and a peak at 1076 cm^{-1} for a secondary hydroxyl group. In the nanoparticles, the chitosan peaks at 3415 cm^{-1} and 1653 cm^{-1} were combined with the alginate peaks and shifted to 3408 cm^{-1} and 1577 cm^{-1}, respectively. The characteristic peak near 1419 cm^{-1} was attributed to the ionic interaction between alginate and chitosan.[36]

The DSC thermograms of alginate, chitosan, meloxicam, and the nanoparticles were also analyzed [Figure 6(b)]. Alginate and chitosan had exothermic peaks at 240°C and 295°C, respectively. The endothermic peaks were attributed to the loss of water, and the exothermic peaks appeared due to the degradation caused by the decarboxylation and oxidation of the polymers. Meloxicam had an endothermic peak at 252°C and an exothermic peak at 268°C. In meloxicam-loaded nanoparticles, the exothermic peaks of alginate and chitosan disappeared, and an endothermic peak at 302.8°C was obtained, most likely indicating an interaction between two polymers.

In Vitro Release Studies and Release Kinetic Models

The maximum meloxicam release in the formulations containing 0.15% drug (formulations 7, 8, 11, and 12) ranged between 15 and 25%, which was lower than the other formulations. The

Table III. Composition of Checkpoint Formulations, the Predicted and Experimental Values of Response Variables and Percentage Prediction Error

Optimized formulation composition ($X_1 : X_2 : X_3$)	Response variable	Experimental value	Predicted value	Percentage Prediction error
6.6 :0.05 :0.05	Y_1 (nm)	283	262	−7.4
	Y_2 (mV)	−16.9	−17.9	5.9
	Y_3 (%)	55	53	−3.6
	Y_4 (h)	8.9	8.4	−5.5
5.7 :0.04 :0.08	Y_1 (nm)	274	271	−1
	Y_2 (mV)	−18.1	−18.3	1.1
	Y_3 (%)	50	52	4
	Y_4 (h)	8.6	9	4.6
3 :0.05 :0.05	Y_1 (nm)	386	371	−3.8
	Y_2 (mV)	−23.7	−24.8	4.6
	Y_3 (%)	35.8	37.7	5.3
	Y_4 (h)	11	11.5	4.5

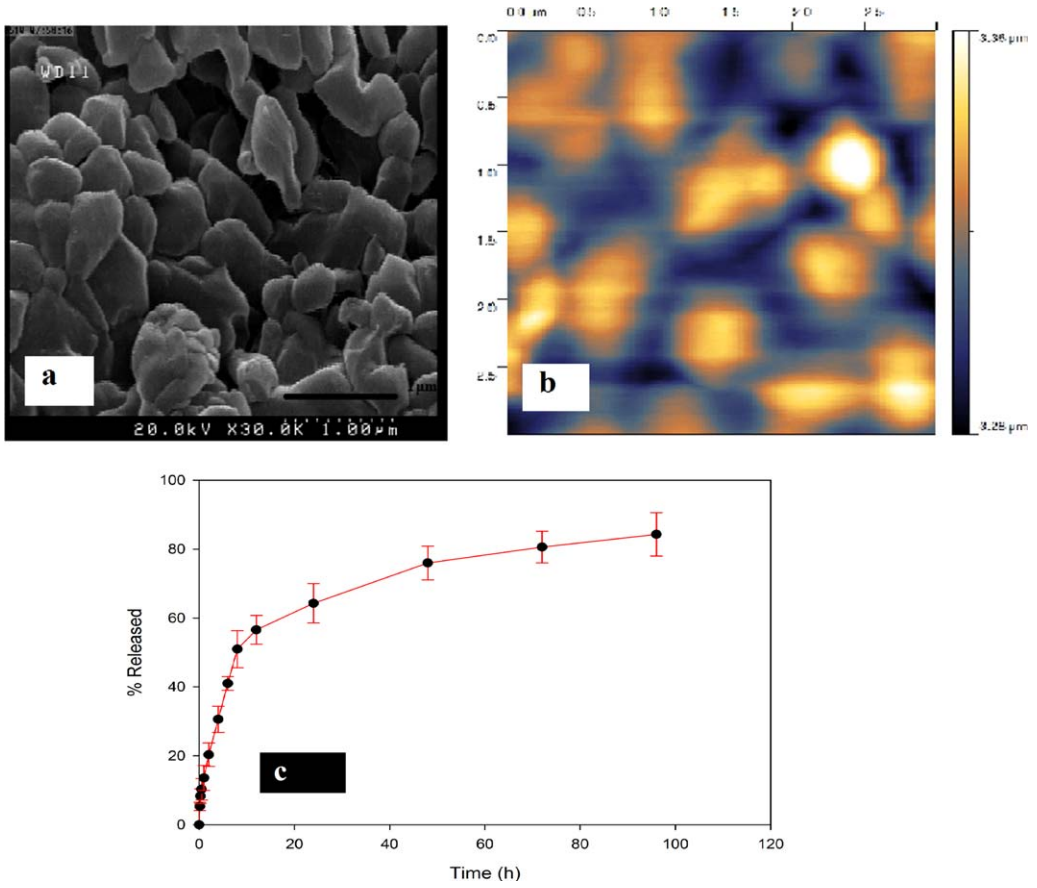

Figure 5. (a) FESEM and (b) AFM photomicrographs of meloxicam-loaded nanoparticles and (c) in vitro meloxicam release profile of the optimized formulation, ($n = 3$, bars represent SD). [Color figure can be viewed in the online issue, which is available at wileyonlinelibrary.com.]

amount of drug released in formulations 1, 2, 3, and 4 with 0.1% meloxicam was 28−41%, and formulations 5, 6, 9, and 10 with 0.05% meloxicam had higher releases (52−61%) due to the reasons previously discussed, demonstrating that the meloxicam concentration had a great effect on MDT and release. In formulations 13, 14, and 15 with a 0.1% meloxicam concentration, the release was also high (65−71%). The released amount was almost equal to formulations 5, 6, 9, and 10, although the last formulations had a rapid slope in the first release stage, and the former formulations had a mild release (Figure 4). These results may be due to better drug entrapment in formulations 13, 14, and 15. Additionally, the variable values for the

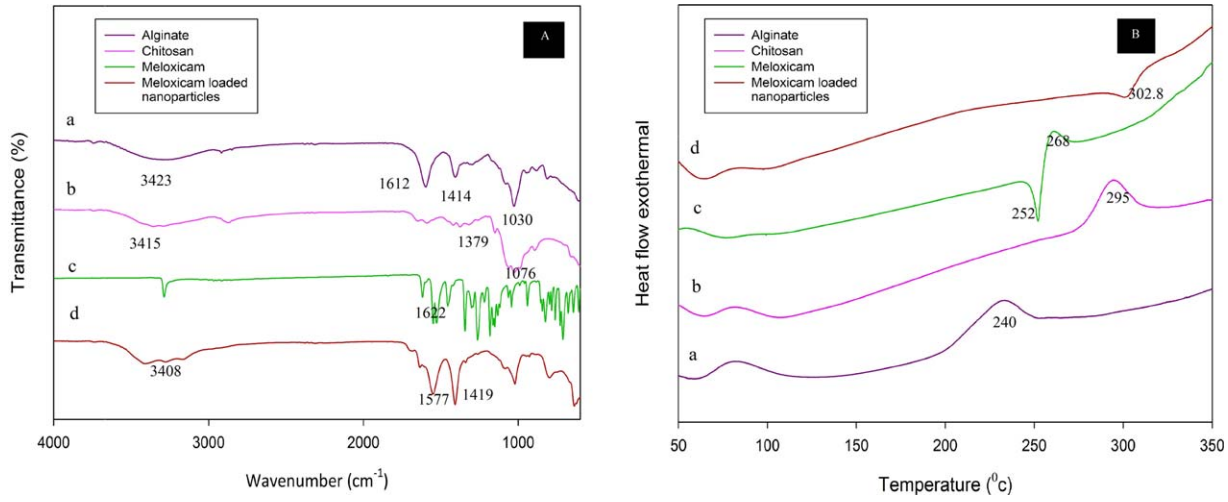

Figure 6. (A) The ATR-FTIR spectra and (B) the DSC thermograms of (a) alginate, (b) chitosan, (c) meloxicam, and (d) meloxicam loaded nanoparticles. [Color figure can be viewed in the online issue, which is available at wileyonlinelibrary.com.]

optimum formulation offered by the software were close to the empirical values in these formulations. The *in vitro* release study for the optimized formulation in PBS containing 0.5% Tween 20, with pH 7.4, is shown in Figure 5(c). The release profile was characterized by two steps. In the first step, over 8 h, almost 51% of the drug was released, and at 96 h, the sustained release phase, almost 85% of drug was released. The initial release encompasses the surface and near surface associated drug as well as the rapid hydration of nanoparticles due to the hydrophilic nature of chitosan and alginate. Then, the medium penetrates into the nanoparticles, and the entrapped drug dissolves and gradually diffuses, delaying the drug release.

The values of the regression coefficients for the Zero order, Higuchi, First order, Hixon-Crowell and Korsmeyer-Peppas models were 0.960, 0.981, 0.977, 0.969, and 0.990, respectively. An examination of the regression coefficients indicated that the Higuchi model was the best fitted model to the release kinetics. The Higuchi model accounts for the polymer swelling, transition of the polymers from the glassy to the rubbery state, polymer dissolution and drug diffusion. This model describes a diffusion controlled model from a porous matrix. The release exponent, *n*, was determined to be 0.586, demonstrating a non-Fickian release mechanism, which refers to both diffusion and swelling.[46]

CONCLUSIONS

The entrapment of a hydrophobic drug entity, meloxicam, was successfully performed in alginate-chitosan-pluronic nanocomposites. The nanoparticles were designed using Box-Behnken experimental design and were optimized. The best fitted model was the quadratic model for all evaluated responses. The R^2 for Y_1, Y_2, Y_3, and Y_4 was 0.9873, 0.9632, 0.9780, and 0.9885, respectively. The adjusted R^2 was 0.9475, 0.8969, 0.9384, and 0.9678, respectively. Consequently, an increase in the alginate to chitosan mass ratio led to a decrease in the particle size. The alginate to chitosan mass ratio had the greatest effect on zeta potential. A decrease in meloxicam concentration resulted in an increase in EE and a decrease in the MDT. This novel formulation may be used as a sustained release dosage form in an injectable hydrogel base for osteoarthritis treatment.

ACKNOWLEDGMENTS

This work was supported by research grant No.290367 from Isfahan Pharmaceutical Sciences Research Centre of the Isfahan University of Medical Sciences and Isfahan University of Technology. Authors gratefully appreciate Dr Behshid Behdadfar's assistance. The authors also thank Miss Elaheh Moazeni for her cooperation.

REFERENCES

1. Motwani, S. K.; Chopra, S.; Talegaonkar, S.; Kohli, K.; Ahmad, F. J.; Khar, R. K. *Eur. J. Pharm. Biopharm.* **2008**, *68*, 513.
2. Bang, S. H.; Yu, Y.; Hwang, C.; Park, H. J. *J. Microencapsul.* **2009**, *26*, 722.
3. Stoop, R. *Injury.* **2008**, *39* (Suppl 1), 77.
4. Gerwin, N.; Hops, C.; Lucke, A. *Adv. Drug Del. Rev.* **2006**, *58*, 226.
5. Kurti, L.; Gaspar, R.; Marki, A.; Kapolna, E.; Bocsik, A.; Veszelka, S.; Bartos, C.; Ambrus, R.; Vastag, M.; Deli, M. A.; Revesz, P. S. *Eur. J. Pharm. Sci.* **2013**, *50*, 86.
6. Douglas, K.; Tabrizian, M. *J. Biomater. Sci.* **2005**, *16*, 43.
7. Hamidi, M.; Azadi, A.; Rafiei, P. *Adv. Drug Del. Rev.* **2008**, *60*, 1638.
8. Turkoglu, T.; Tascıoglu, S. *J. Appl. Polym. Sci.* **2014**, 131.
9. Kasoju, N.; Bora, U. *J. Biomater. Mater. Res Part B.* **2012**, *100*, 1854.
10. Zhou, X.; Cheng, X. J.; Liu, W. F.; Li, J.; Ren, L. H.; Dang, Q. F.; Feng, C.; Chen, X. G. *J. Appl. Polym. Sci.* **2013**, 127.
11. Hosseini, S. F.; Zandi, M.; Rezaei, M.; Farahmandghavi, F. *Carbohydr. Polym.* **2013**, *95*, 50.
12. Domaratzki, R.; Ghanem, A. *J. Appl. Polym. Sci.* **2013**, *128*, 2173.
13. Sahu, A.; Goswami, P.; Bora, U. *J. Mater. Sci: Mater. Med.* **2009**, *20*, 171.
14. Aquino, R.; Auriemma, G.; Amore, M.; D'Ursi, A.; Mencherini, T.; Del Gaudio, P. *Carbohydr. Polym.* **2012**, *89*, 740.
15. Tan, H.; Chu, C. R.; Payne, K. A.; Marra, K. G. *Biomaterials* **2009**, *30*, 2499.
16. Shaji, J.; Varkey., D. *J. Pharmaceutical Invest.* **2013**, *43*, 405.
17. Khalil, R. M.; Abd-Elbary, A.; Kassem, M. A.; Ghorab, M. M.; Basha, M. *Pharm. Dev. Technol.* **2014**, *19*, 304.
18. Khurana, S.; Jain, N. K.; Bedi, P. M. S. *Life Sci.* **2013**, *92*, 383.
19. Şengel-Türk, C. T.; Hasçiçek, C.; Dogan, A. L.; Esendagli, G.; Guc, D.; Gönül, N. *Drug Dev. Ind. Pharm.* **2012**, *38*, 1107.
20. Albuquerque, B.; Costa, M. S.; Peça, I. N.; Cardoso, M. M. *Polym. Eng. Sci.* **2013**, *53*, 146.
21. Ianiski, F. R.; Alvesa, C. B.; Souza, A. C. G.; Pinton, S.; Roman, S. S.; Rhoden, C. R. B.; Alves, M. P.; Luchese, C. *Behav. Brain Res.* **2012**, *230*, 100.
22. Yadav, N.; Khatak, S.; Sara, U. S. *Int. J. Appl.* **2013**, *5*, 8.
23. Butoescu, N.; Jordan, O.; Petrifink, A.; Hofmann, H.; Doelker, E. *J. Microencapsul.* **2008**, *25*, 339.
24. Danhier, F.; Ansorena, E.; Silva, J. M.; Coco, R.; Breton, A. L.; Préat, V. *J. Control. Release* **2012**, *161*, 505.
25. Shinde, N. C.; Keskar, N. J.; Argade, P. D. *Res. J. Pharma. Biol. Chem. Sci.* **2012**, *3*, 922.
26. Rajaonarivonyc, M.; Couarrazfe, V.; Couvreur, P. *J. Pharm. Sci.* **1993**, *82*, 912.
27. Finotelli, P. V.; Silva, D. D.; Sola-Penna, M.; Rossi, A. M.; Farina, M.; Andrade, L. R.; Takeuchi, A. Y.; Rocha-Leão, M. H. *Colloids Surf. B Biointerfaces* **2010**, *81*, 206.
28. Martínez, A.; Iglesias, I.; Lozano, R.; Teijónc, J. M.; Blancoc, M. D. *Carbohydr. Polym.* **2011**, *83*, 1311.
29. Ramana, L. N.; Sharma, S.; Sethuraman, S.; Ranga, U.; Krishnan, U. M. *Biochim. Biophys. Acta* **2014**, *1840*, 476.
30. Dash, S.; Murthy, P. N.; Nath, L.; Chowdhury, P. *Acta Poloniae Pharmaceutica ñ Drug Research.* **2010**, *67*, 217.

31. Ping, L.; YaNi, D.; JunPing, Z.; AiQin, W.; Qin, W. *Int. J. Biomed. Sci.* **2008**, *4*, 221.
32. Xing, J.; Deng, L.; Dong, A. *J. Appl. Polym. Sci.* **2010**, *117*, 2354.
33. Batrakova, E. V.; Kabanov, A. V. *J. Control. Release* **2008**, *130*, 98.
34. Escobar-Chávez, J. J.; López-Cervantes, M.; Naïk, A.; Kalia, Y. N.; Quintanar-Guerrero, D.; Ganem-Quintanar, A. *J. Pharm. Pharma. Sci.* **2006**, *9*, 339.
35. Batrakova, E. V.; Kabanov, A. V. *J. Control. Release* **2008**, *130*, 98.
36. Das, R.; Kasoju, N.; Bora, U. *Nanomedicine* **2010**, *6*, 153.
37. Simsek-Ege, F. A.; Bond, G. M.; Stringer, J. *J. Appl. Polym. Sci.* **2002**, *88*, 346.
38. Chen, S.; Liu, M.; Jin, S.; Wang, B. *Int. J. Pharma.* **2008**, *349*, 180.
39. Sood, S.; Jain, K.; Gowthamarajan, K. *Colloids Surf. B Biointerfaces* **2014**, *113*, 330.
40. Li, G. Y.; Zhong, M.; Zhou, Z. D.; Zhong, Y. D.; Ding, P.; Huang, Y. *Int. J. Biol. Macromol.* **2011**, *49*, 970.
41. Dong, Y.; Feng, S. S. *Biomaterials* **2004**, *25*, 2843.
42. Villar, A. M. S.; Naveros, B. C.; Campmany, A. C. C.; Trenchs, M. A.; Rocabert, C. B.; Bellowa, L. H. *Int. J. Pharm.* **2012**, *431*, 161.
43. Liu, J.; Hu, H.; Xu, J.; Wen, Y. *Bioresources* **2012**, *7*, 2121.
44. Ming, J. W.; Yu, L. X.; Zheng, J. C.; Shan, J. Y. *J. Appl. Polym. Sci.* **2010**, *117*, 3001.
45. Shalviri, A.; Chan, H. K.; Raval, G.; Abdekhodaie, M. J.; Liu, Q.; Heerklotz, H.; Wu, X. Y. *Colloids Surf. B Biointerfaces* **2013**, 101.
46. Siepmann, J.; Peppas, N. *Adv. Drug Del. Rev.* **2001**, *48*, 139.